Reports

X-ray Standing Waves: A Molecular Yardstick for Biological Membranes

M. J. BEDZYK, D. H. BILDERBACK, G. M. BOMMARITO,
M. CAFFREY, J. S. SCHILDKRAUT

Structural information on an atomic scale has been obtained for a Langmuir-Blodgett (LB) trilayer system by means of long-period x-ray standing waves. The LB trilayer of zinc and cadmium arachidate was deposited on a layered synthetic microstructure (LSM) consisting of 200 tungsten/silicon layer pairs with a 25 Å period. A 30 Å thermally induced inward collapse of the zinc atom layer that was initially located in the LB trilayer at 53 Å above the LSM surface has been observed. The mean position and width of the zinc atom layer was determined with a precision of ±0.3 Å.

LANGMUIR-BLODGETT (LB) FILM PRODUCTION was first reported on in the early 1930s. Since then, interest in these ultrathin assemblies has grown as a result of potential applications in such diverse areas as electronics, optoelectronics, optics, catalysis, filtration, diffusion, energy conservation, and biosensing. Biologically, LB films have been extensively used as models for biomembranes. A number of techniques have been used to probe the molecular structure of such membrane films. The most detailed information is derived from neutron diffraction and magnetic resonance studies used in combination with selectively deuterated amphiphiles (*1–3*). In the former case, the mean positions of the labeled chain segments in both solid and fluid lipid bilayers were derived with a resolution of 6 Å. With the exception of single crystal diffraction measurements, to our knowledge this represents the highest position resolution available to date. Herein, we describe an approach that uses x-ray standing waves for determining the position $\langle z \rangle$ and width $\langle z^2 \rangle^{1/2}$ of heavy atom layers in LB films with subangstrom accuracy.

An x-ray standing wave can be generated by the interference between two coherently related x-ray beams. Conventional x-ray standing-wave measurements (*4–9*) use dynamical Bragg diffraction (*10*) from perfect single crystals for generating x-ray standing-wave probes with *d*-spacing periods ranging from 1 to 4 Å (Fig. 1). This technique, which was first applied to the study of implanted layers (*4–6*), reached a new level of interest when it was realized (*6*) that the standing wave extended above the surface, and could therefore be used for examining adsorbed surface layers (*7–9*). Such measurements have proven to be very precise in determining where, and how well, impurity atom distributions register with respect to the perfect crystal diffraction planes. This information, which is obtained by observing the modulation in the impurity atom fluorescence yield as the standing-wave antinodes shift inward by one-half of a *d*-spacing during a scan in angle θ through the Bragg reflection, would also be useful for studying the layered arrangement of atoms in LB films. However, the characteristic modulo-*d* length scale of a few angstroms, which makes this technique so appropriate for studying bond length distances between atom layers at single crystal surfaces, is too short for measuring the spacing between heavy atom layers in LB films. For this reason we have chosen to use x-ray standing waves with periods ranging from 20 to 200 Å to better match the thickness of LB films of biologically relevant materials.

As recently demonstrated, such long-period x-ray standing waves can be generated by Bragg diffraction from layered synthetic microstructures (LSMs) (*11–13*) or by total external reflection from mirror surfaces (*14*). Herein, we describe the use of both of these techniques for characterizing the thermotropic order/disorder transition in a metal soap film (Fig. 2).

For Bragg diffraction purposes, an LSM is fabricated as a depth-periodic layered structure consisting of 10 to 200 layer pairs of alternating high and low electron density materials (such as tungsten and silicon or platinum and carbon) (*15*). Sufficient uniformity of the layer thicknesses can be maintained in the range between 10 and 100 Å. The corresponding fundamental diffraction plane spacing can therefore be from *d* = 20 to 200 Å. Owing to the low number of layer pairs that effect Bragg diffraction, these optical elements have a rather large x-ray energy bandpass and angular reflection width. The quality of LSMs is such that experimental Bragg reflection curves compare well with dynamical diffraction theory, and peak reflectivities are as high as 80%. Therefore, a well-defined standing wave can be generated and used to probe structures deposited on an LSM surface with a periodic scale equivalent to this rather large *d*-spacing. With the capability of choosing both the standing-

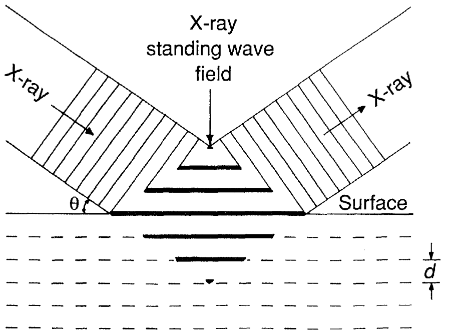

Fig. 1. Illustration of the x-ray standing-wave field formed by the interference between the incident and Bragg-diffracted x-ray plane waves. Tilting angle θ through the narrow reflection condition causes the antinodes of the standing wave to shift inward by one-half of a diffraction-plane spacing *d*.

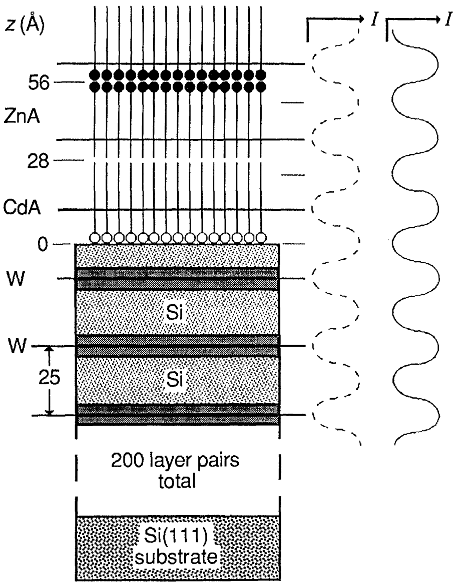

Fig. 2. Schematic showing fully extended untilted zinc/cadmium arachidate LB layers deposited on the plasma-cleaned silicon surface of a W/Si LSM with a 25 Å *d*-spacing. The standing wave generated on the low (- - -) and high (——) angle side of the Bragg reflection are depicted along the right side.

M. J. Bedzyk and D. H. Bilderback, Cornell High Energy Synchrotron Source (CHESS) and School of Applied and Engineering Physics, Cornell University, Ithaca, NY 14853.
G. M. Bommarito, Department of Chemistry, Cornell University, Ithaca, NY 14853.
M. Caffrey, Department of Chemistry, Ohio State University, Columbus, OH 43210.
J. S. Schildkraut, Corporate Research Laboratories, Eastmen Kodak Company, Rochester, NY 14650.

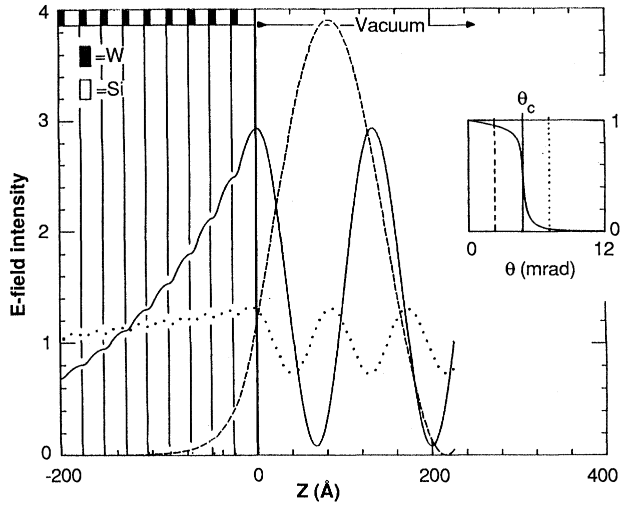

Fig. 3. The height z dependence of the normalized E-field intensity generated during specular reflection of a 9.8-keV x-ray plane wave from the surface of the W/Si LSM shown in Fig. 2. The dashed line is for $\theta = (1/2)\theta_c$. The solid line is for $\theta = \theta_c$. The dotted line is for $\theta = (3/2)\theta_c$. Specular reflectivity versus angle θ is shown in the inset for this case.

wave period and material composition used in the LSM, this technique has great potential for resolving various surface and interface structures.

Because x-ray frequencies are greater than the natural frequencies for most bound electrons in matter, the refractive index for x-rays is less than unity. Therefore, if the incident angle at an optical boundary is smaller than the critical angle, x-rays will undergo total external reflection, in an analogous way to visible light undergoing total internal reflection.

Not only can an x-ray standing wave be generated by the interference between the incident and Bragg-diffracted traveling plane waves (Fig. 1), but a standing wave can also be generated by the interference between the incident and specularly reflected traveling plane waves. During specular (or total external) reflection, the x-ray standing wave is formed in the more optically dense medium above the mirror surface, and an evanescent (or exponentially damped) wave is formed below the mirror surface with a very short penetration depth into the less optically dense medium. Although much attention has been given to the evanescent wave (*16–18*) (with applications to surface diffraction and surface-enhanced fluorescence), the long-period property of this standing wave has not been utilized until now for structure determination.

During Bragg diffraction, the standing-wave nodes coincide with the diffraction planes on the low-angle side of the strong reflection condition, and as the angle θ is increased through the strong reflection condition, the standing wave moves inward until the antinodes reach the diffraction planes (Fig. 2). To a good approximation, the first-order Bragg diffraction planes coincide with the centers of the heavy atom layers in the LSM. Above the surface of the LSM the period (D) of the standing wave is simply related to the wavelength λ and angle 2θ between the two interfering plane waves as

$$D = \lambda/(2\sin\theta) \tag{1}$$

As the standing wave moves inward, the fluorescence yield from a layer of heavy atoms sitting above the LSM surface will show a characteristic modulation. The phase of this modulation (or coherent position) is a measure of the atom layer's average position $\langle z \rangle$ modulo the d-spacing of the LSM. The amplitude of this modulation (or coherent fraction) is a measure of the width of the atom layer, $\langle z^2 \rangle^{1/2}$. If all of the heavy atoms were contained in a plane, which was parallel to the diffraction planes, the coherent fraction would equal unity. On the other hand, if the heavy atoms were randomly distributed in a very thick overlayer, the coherent fraction would be zero.

Standing waves under the total external reflection condition can best be understood by realizing that this specular reflection condition is the zeroth-order Bragg diffraction condition with a diffraction plane at the mirror surface and an infinite d-spacing. Analogous to the above description for normal Bragg diffraction, a standing-wave node lies at the mirror surface at the low-angle side of the strong specular reflection condition (that is, at $\theta = 0$) with the first antinode infinitely far above the mirror surface. As the incident angle θ is advanced through the reflection, the first antinode moves inward until it coincides with the mirror surface at the critical angle θ_c. The remaining antinodes of the standing wave follow behind like a compressing bellows as θ increases with a period of $D = \lambda/(2\sin\theta)$. Advancing above θ_c, the first antinode remains at the mirror surface while the amplitude of the standing wave dies off very rapidly because of the abrupt reduction in intensity of the specularly reflected plane wave.

The standing waves generated at $\theta = (1/2)\theta_c$, θ_c, and $(3/2)\theta_c$ during specular reflection of a 9.8 keV x-ray plane wave from the W/Si LSM used in this study are shown in Fig. 3. The method (*19*) used to calculate these curves (and the first-order Bragg diffraction curves to be shown later) makes use of Parratt's (*20*) recursion formulation with Fresnel coefficients. In our experiment, we scan in angle θ and simultaneously monitor the reflectivity and the fluorescence yields from atoms sitting on, or above, the surface. Because the photoelectric effect is proportional to the electric field intensity at the center of an atom, the variation in electric field intensity predicted from this calculation can be used in comparison to our fluorescence yields to determine how far an atom sits above the reflecting surface. This length scale, which is inherently longer than the first-order Bragg standing-wave period from our LSM, has proven to be invaluable in this study for removing the modulo-d ambiguity from the first-order Bragg results.

Heavy atom soaps have long been used in fabricating stable LB films and as models for biological membranes. They were the obvious choice as a starting material in this work, because they contain an integral heavy atom that can be selected from a large list of metals, which can yield easily detected fluorescence signals. In the present study a marker layer of cadmium arachidate (CdA, a

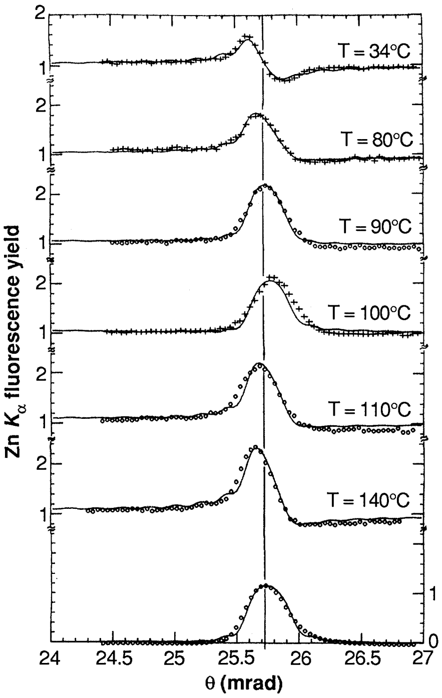

Fig. 4. The experimental (circles) and theoretical (solid line) Bragg reflectivity (bottom curve) at $E_\gamma = 9.8$ keV for the $d = 25$ Å W/Si LSM described in Fig. 2 along with the normalized experimental and theoretical Zn K_α fluorescence yields taken at selected temperatures.

Fig. 5. The experimental and theoretical angular dependence at $E_\gamma = 9.8$ keV of the specular reflectivity, R (Δ), the Zn K_α fluorescence yield at $T = 34°C$ (■) and at $T = 120°C$ (○). The fluorescence yield theory curves correspond to $z = 53$ Å for 34°C and $z = 23$ Å for $T = 120°C$.

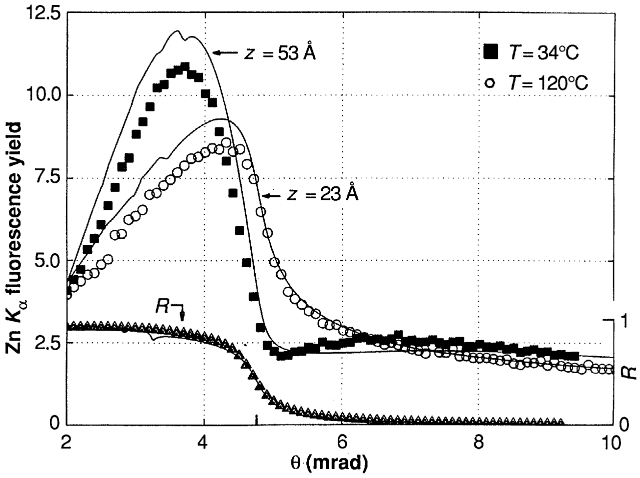

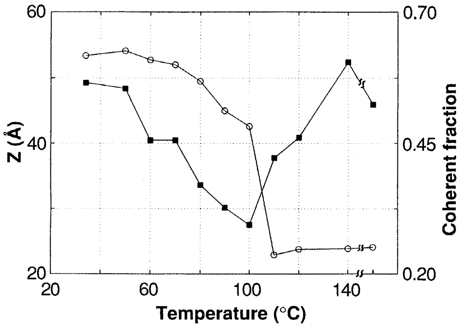

Fig. 6. Experimental summary showing the temperature dependence of the position z (○) of the Zn layer above the LSM surface and the coherent fraction f_c (■) of the Zn layer. From the χ^2 fits shown in Fig. 4, the standard deviations for parameters z and f_c are 0.3 Å and 0.02, respectively. Equation 2 can be used to relate the Zn layer thickness to f_c. Last data points on right-hand side are z and f_c after cooling to 34°C and storage for 8 hours.

C_{20} fatty acid) was laid down in registry with the plasma-cleaned Si surface of a W/Si LSM ($d = 25$ Å with the W thickness $t_W = d/4$). This was followed by the deposition of a zinc arachidate (ZnA) bilayer as depicted schematically in Fig. 2. This arrangement enables the standing-wave analysis to provide a z separation between the two heavy atom types and eliminates the need to know the absolute position of the LSM surface relative to the LSM diffracting planes.

The experiment was carried out at the Cornell High Energy Synchrotron Source (CHESS) with the Cornell Electron Storage Ring (CESR) operating at an electron energy of 5.1 GeV and beam current of 40 to 60 mA. The bending magnet radiation was monochromated by a pair of symmetrically cut Si(111) crystals to x-ray energies (E_γ) of 9.8 and 29 keV for optimally exciting K fluorescence from Zn and Cd, respectively. Both the monochromator and LSM were set up to reflect in the vertical plane. The 10-mm-wide by 25-mm-long LSM was exposed to an incident beam that had a width of 8 mm and a height of 0.1 mm for the Bragg scans and a height of 0.04 mm for the specular scans. An energy-dispersive solid-state detector was positioned perpendicular to the incident beam to collect the fluorescence at a glancing angle with respect to the surface. The LSM was maintained in a helium-filled oven with a temperature stability of ±1°C. Bragg and specular standing-wave scans for Zn were made at 10°C temperature intervals between 35°C and 140°C. Representative scans, which took ~15 min each, are shown in Figs. 4 and 5. The same measurements at a conventional x-ray tube source would have taken ~100 times longer.

The measured coherent position for the Cd layer indicated that the top Si layer of the LSM had been reduced from 18.75 Å to 9.8 Å in thickness by the plasma-cleaning process. This assumes a 1.5 Å radius for the Cd atoms. The Cd coherent position was unaffected by the heating and cooling treatments. The initial 34°C Bragg and specular standing-wave measurements placed the Zn layer at 53.4 Å above the LSM surface, which is slightly shorter than the value of 56 Å for untilted fully extended chains (Fig. 2). The data in Fig. 4 reveal a steady phase advance for the Zn fluorescence modulation as the temperature increases from 34°C to 100°C. At 34°C, the Zn signal peaks on the low-angle side of the Bragg reflection. While at 100°C, the peak has shifted to the high-angle side. This corresponds to a gradual inward movement of the Zn layer by almost one-half of a 25 Å d-spacing. Between 100°C and 110°C the peak in the Zn yield shifts back toward the low-angle side indicating that the Zn has either moved away from the LSM surface by ~(1/4)d or toward it by ~(3/4)d. The specular standing-wave measurement for Zn (Fig. 5) shows that this was in fact a large inward shift. The measurements taken above 110°C revealed no further shift of the Zn layer position. The Zn layer remained at this same inwardly contracted position after cooling to 34°C and waiting for more than 8 hours.

A summary of the thermotropic transition for this LB trilayer system in terms of both the computed Zn layer average position $\langle z \rangle$ above the LSM surface and coherent fraction f_c is given in Fig. 6. These two standing wave–determined parameters are directly related to the projection of the Zn atom distribution along the z-axis. If this distribution were Gaussian with a width $w = 2\langle z^2 \rangle^{1/2}$, then the coherent fraction would be

$$f_c = \exp(-2\pi^2\sigma^2) \qquad (2)$$

where $\sigma = w/(2D)$. This Debye-Waller factor–like model (*9*) predicts that the projected Zn layer has a width $w = 7.9$ Å for the maximum measured Zn coherent fraction of $f_c = 0.61$ and a width $w = 11.8$ Å for the minimum $f_c = 0.33$. Considering that Zn atom positions from an area of 30 mm^2 were projected into this distribution, the narrowness of this width is quite remarkable and attests to the uniform thickness of both the top Si layer and the LB layers.

The initial Zn layer position of $z = 53.4$ Å at 34°C (Fig. 6) is very close to the expected value, given a slight tilting (17.5°) of the acyl chains. In fact, x-ray scattering measurements (*21*) give 54 Å as the bilayer spacing for LB multilayers of Cd arachidate. The gradual movement of the Zn layer toward the LSM surface in the 70°C to 100°C range along with the decrease in coherent fraction (that is, increase in Zn layer width) suggests a premelting phenomenon. The precipitous inward collapse of the Zn layer between 100°C and 110°C is paralleled by a significant increase in the Zn layer coherent fraction in this same temperature range. Continued heating to 140°C does not alter the position of the zinc layer. This aspect of the transition is irreversible upon cooling to 34°C and incubation at this temperature for >8 hours. In contrast to the Zn layer position, the Zn coherent fraction continues to rise with temperature from 110°C to 140°C, indicating a further reduction in the width of the Zn layer. This is followed by a slight increase in width upon cooling to and subsequent storage for 8 hours at 34°C. After this thermal cycling, the phase of the Cd standing-wave profile did not change, although a decrease in coherent fraction from 0.50 to 0.34 was observed. This suggests that the Cd layer was still in registry with the LSM surface and that perhaps some disordering had occurred to slightly increase the spread of this interfacial layer.

The thermotropic properties of bulk samples and multilamellar LB films composed of pure heavy-atom soaps have been studied in some depth (*22–26*). However, because the present LB sample is a solid supported trilayer and is heterogeneous, consisting of a CdA monolayer and a ZnA bilayer, comparison with the aforementioned systems, although instructive, is not rigorous. At low temperatures, the dry powdered CdA exists in a lamellar (smectic) phase with rigid hydrocarbon chains densely packed in a crystalline arrangement, their long axis oriented normal to the bilayer surface. At 120°C, the chains undergo a conformation order/disorder transition accompanied by a transformation from lamellar to hexagonal long-range order. This high-temperature phase is of the inverted hexagonal type and it persists upon heating up to 220°C (*23*). To our knowledge no such information is available in the literature concerning the thermotropic phase properties of ZnA.

It is interesting to note that in the present mixed trilayer system a dramatic change in both the Zn-Cd separation and in the coherent fraction of Zn occurred close to the major thermotropic transition temperature observed in bulk CdA (*23*). However, because the standing wave method does not provide a direct determination of the molecular structure of the low electron density (carbonaceous) material in the assembly, one can only speculate on the underlying structural changes in the hydrocarbon core and polar headgroups of the trilayer that accompany this Zn shift. For example, this shift could be accounted for by one or a combination of the following events: hydrocarbon chain "melting," tilting, and/or interdigitation. In the present system, chain melting alone would contribute a shift of only 7 Å based on model calculations. Tilting alone, on the other hand, would require a 62.9° deviation of the long axis of the soap molecule from the normal to the planar surface to effect the measured 30.4 Å total reduction in the Zn-Cd separation. Such extreme tilting requires that a large number of methylene groups are taken out of van der Waals contact, which would prove to be an energetically expensive proposition. In contrast, interdigitation alone could account for a 28 Å shift since the hydrocarbon chain length of arachidate in its fully extended form is 28 Å and complete interdigitation of the chains is a distinct possibility. As noted previously, the observed shift may also come about from a combination of the above. The gradual "pretransitional" reduction in Zn-Cd separation could similarly be explained. It seems unlikely that the hexagonal phase is involved in the transition owing to a paucity of material in the LB film. It is possible that the fall in coherent fraction in the vicinity of 100°C derives from a coexistence in the same monolayer of soap molecules of the low- and high-temperature configuration.

REFERENCES AND NOTES

1. G. Zaccai, G. Buldt, A. Seelig, J. Seelig, *J. Mol. Biol.* **134**, 693 (1979).
2. A. Seelig and J. Seelig, *Biochemistry* **13**, 4839 (1974).
3. E. Oldfield, M. Meadows, D. Rice, R. Jacobs, *ibid.* **17**, 2727 (1978).
4. B. W. Batterman, *Phys. Rev.* **133**, A759 (1964).
5. J. A. Golovchenko, B. W. Batterman, W. L. Brown, *Phys. Rev. B* **10**, 4239 (1974).
6. S. K. Andersen, J. A. Golovchenko, G. Mair, *Phys. Rev. Lett.* **37**, 1141 (1976).
7. P. L. Cowan, J. A. Golovchenko, M. F. Robbins, *ibid.* **44**, 1680 (1980).
8. J. A. Golovchenko, J. R. Patel, D. R. Kaplan, P. L. Cowan, M. J. Bedzyk, *ibid.* **49**, 560 (1982).
9. M. J. Bedzyk and G. Materlik, *Phys. Rev. B* **31**, 4110 (1985).
10. M. von Laue, *Roentgenstrahlinterenzen* (Akademische Verlagsgesellshaft, Frankfurt a.M., 1960). For a review, see B. W. Batterman and H. Cole, *Rev. Mod. Phys.* **36**, 681 (1961).
11. T. W. Barbee and W. K. Warburton, *Mater. Lett.* **3**, 17 (1984).
12. M. J. Bedzyk, D. Bilderback, J. White, H. D. Abruna, M. G. Bommarito, *J. Phys. Chem.* **90**, 4926 (1986).
13. T. Matsushita, A. Iida, T. Ishikawa, T. Nakagiri, K. Sakai, *Nucl. Instrum. Meth.* **A246**, 751 (1986).
14. M. J. Bedzyk, *ibid.* **A266**, 679 (1988).
15. D. H. Bilderback, B. M. Lairson, T. W. Barbee, G. E. Ice, C. J. Sparks, *ibid.* **208**, 251 (1983).
16. W. C. Marra, P. Eisenberger, A. Y. Chou, *J. Appl. Phys.* **50**, 6927 (1979).
17. R. S. Becker, J. A. Golovchenko, J. R. Patel, *Phys. Rev. Lett.* **50**, 153 (1983).
18. J. M. Bloch *et al.*, *Phys. Rev. Lett.* **54**, 1039 (1985).
19. M. J. Bedzyk and G. M. Bommarito, in preparation.
20. L. G. Parratt, *Phys. Rev.* **95**, 359 (1954).
21. P. Fromherz, U. Oelschlagel, W. Wilke, paper presented at the Third International Conference on Langmuir-Blodgett Films, Göttingen, 26 July 1987.
22. P. P. A. Spegt and A. E. Skoulios, *Acta Cryst.* **16**, 301 (1963).
23. R. D. Vold and G. S. Hattiangdi, *Ind. Engin. Chem.* **41**, 2311 (1949).
24. G. S. Hattiangdi *et al.*, *ibid.*, p. 2320.
25. I. Naselli, J. F. Rabolt, J. D. Swalen, *J. Chem. Phys.* **82**, 2136 (1985).
26. D. D. Saperstein, *J. Phys. Chem.* **90**, 1408 (1986).

27. This work was supported by the National Science Foundation (DMR-84-12465) and by the National Institutes of Health (DK36849, HL18255, and RR01646).

22 April 1988; 2 August 1988

Single Strands, Triple Strands, and Kinks in H-DNA

HAN HTUN AND JAMES E. DAHLBERG

A naturally occurring (dT-dC)$_{18}$:(dA-dG)$_{18}$ repeat in the H conformation of DNA was shown to contain single-stranded nucleotides in the center of the TC$_{18}$ repeat and on one half of the AG$_{18}$ repeat. These results support the model that H-DNA is a structure containing both triple-stranded and single-stranded regions. The stability of this structure was affected by both *p*H and the degree of negative supercoiling: at *p*H 7.6 to 7.7, a high level of supercoiling was needed to keep about half of the molecules in the H conformation; at *p*H 6 and *p*H 5, normal levels of supercoiling supported H-DNA; and at *p*H 4, no supercoiling was required. At mildly alkaline *p*H, the TC/AG$_{18}$ repeat assumed a novel conformation called J-DNA that differed from both the B and H forms. A three-dimensional model for the structure of H-DNA is proposed that accounts both for the single-strandedness of the nucleotides and for the influence of supercoiling on H-DNA formation. This model predicts and evidence is presented that H-DNA introduces a sharp kink in the DNA. Moreover, the angle of this kink appears not to be fixed, so that H-DNA is also a hinged-DNA.

THE REPEATING COPOLYMER (dT-dC)$_n$:(dG-dA)$_n$ in DNA (TC/AG$_n$) has an unusual structure, as revealed by its sensitivity to single-stranded specific nucleases (*1–7*) and its ability to relax negative supercoils in DNA (*5–8*). The most widely accepted model of this structure contains triple-stranded and single-stranded regions called H-DNA (*9, 10*). The need for symmetry in nucleotide sequence (*11*) and the location of bases that are sensitive to chemical or enzymatic probes (*1–7, 12*) support this model. Because all of the reagents used in those studies can react with bases that are in exposed but not single-stranded structures (*13*), those results are also consistent with other structures that have been proposed, such as self-paired cruciforms or altered double-stranded structures (*3–7, 14, 15*).

Models for the triple-stranded nature of H-DNA were based on earlier studies of mixtures of (dT-dC)$_n$ and (dG-dA)$_n$ oligonucleotides (TC$_n$ and AG$_n$ repeats). A one-to-one mixture of these oligonucleotides formed a triple-stranded helix spontaneously in mild acid, with one AG$_n$ repeat pairing both to a TC$_n$ repeat and to a protonated TC$_n^+$ repeat through Watson-Crick and Hoogsteen base pairs, respectively (*16*); the polypyrimidine strands are antiparallel (*17*). Hence, Lee *et al.* (*9*) and Lyamichev *et al.* (*10*) proposed that this conformation could

---

Department of Physiological Chemistry, University of Wisconsin–Madison, Madison, WI 53706.